Hindawi
International Journal of Antennas and Propagation
Volume 2019, Article ID 3518691, 10 pages
https://doi.org/10.1155/2019/3518691

Research Article

Zero-Forcing Precoding in the Measured Massive MIMO Downlink: How Many Antennas Are Needed?

Zhe Zheng[1], **Jianhua Zhang**[1], **Xiaoyong Wu**[2], **Danpu Liu**[3] **and Lei Tian**[1]

[1]*State Key Laboratory of Networking and Switching Technology, Beijing University of Posts and Telecommunications, Beijing 100876, China*
[2]*Shanghai Radio Equipment Research Institute, Shanghai 200090, China*
[3]*Beijing Laboratory of Advanced Information Network, Beijing University of Posts and Telecommunications, Beijing 100876, China*

Correspondence should be addressed to Jianhua Zhang; jhzhang@bupt.edu.cn

Received 30 October 2018; Accepted 26 February 2019; Published 11 April 2019

Academic Editor: Riccardo Colella

In order to understand how many antennas are needed in a multiuser massive MIMO system, theoretical derivation and channel measurements are conducted; the effect of a finite number of base station (BS) antennas on the performance capability of Zero-forcing (ZF) precoding in a rich scattering channel is quantified. Through the theoretical analysis, the needed number of the transmit antennas for ZF precoder to achieve a certain percentage of the broadcast channel (BC) capacity will monotonically decrease with the increase of the transmit signal-to-noise ratio (SNR), and the lower bound of the needed transmit antennas is derived with a simple expression. Then the theoretical derivation is verified by simulation results, and the transmission performance is evaluated by channel measurements in urban microcell (UMi) scenario with frequencies of 3.5 and 6 GHz. From the measurement results, the ZF capability can be enhanced by improving the SNR and enlarging the antenna array spacing when the massive MIMO channel does not under a favorable propagation condition. Furthermore, because of the lower spatial correlation, the performance of ZF precoding at 6 GHz is closer to the theoretical derivation than 3.5 GHz.

1. Introduction

As the current hot issue, Fifth Generation (5G) New Radio (NR) technology is expected to meet the explosive growth of current mobile data traffic, due to the advantages of higher transmission rate, lower latency, and lower energy consumption compared with existing communication technologies [1]. The key technologies of 5G include massive multi-input and multiple-output (MIMO), mmWave, ultra-densification, and so on [2]. Massive MIMO can fully exploit spatial degrees of freedom by configuring tens or even hundreds of antennas at the base station to improve the spectral efficiency, the multiuser multiplexing, and intercell interference [3], which is regarded as one of the key technologies of 5G NR.

Theoretically, when assuming an infinite number of antennas at the base station (BS), the effect of small-scale fading and thermal noise can be eliminated only remains pilot contamination from other cells, which makes the simplest sort of precoding on the forward link and processing on the reverse link possible [4]. In that way, how many antennas are needed in massive MIMO system?

There are already some precoding investigations considering the antenna number reported in the current literature. In [5], the uplink and downlink of a multicellular TDD system are studied. Under the assumption that the number of antennas per BS and the number of users per cell are large, the asymptotic approximation of the reachable rate is derived and how many antennas are needed to achieve the ultimate performance of η% is analyzed. The authors also suggest it is necessary to verify the theoretical performance predictions by channel measurements and prototypes. In [6], the existence of pilot contamination effects in a multicell multiuser massive MIMO system under the finite-dimensional channel model is studied. Furthermore, the lower bound of the uplink data transmission achievable rate is derived, and the sum rate performances of the MRC and ZF linear receivers are compared.

In [7], the performance of MIMO transmitters under correlation channels is studied. When the number of antennas is increased continuously in a limited fixed physical space, spatial diversity is reduced, but transmission diversity is increased. Through these two contradicting phenomena, the authors found that, by reducing the separations between the antennas to significantly less than the transmit wavelength to fit more antennas, the resulting system performance improves. However, the literature [8] shows that there is an upper bound on the number of antennas required in a limited space. When the upper bound is reached, increasing the number of antennas will cause the inner product of the channel vector to tend to a nonzero value. This means that interference between users does not disappear, creating a saturation effect on the achievable rate.

How many antennas are needed in the actual system to achieve the performance described in the literature [4] is discussed, which is subject to the actual propagation environment.

In [9], a channel measurement in the residential area is carried out to study the linear precoding performance of ZF and MMSE with a very large but limited number of antennas in the realistic propagation environment. It is shown that the orthogonality between channels to different users improves with the increase of the number of antennas in the base station. However, for two single-antenna users, the improvement of orthogonality is no longer obvious when the transmitting antennas are greater than 20.

Several researches have quantified the performance of zero-forcing (ZF) from different aspects. The lower bound of the sum-rate of ZF detection with both perfect channel state information (CSI) and imperfect CSI was derived in [10]. Then the insight that the transmit power of each user can be made inversely proportional to the number of BS antennas while maintaining a desired quality of service was proposed in massive MIMO regime [11]; i.e., *infinite* antenna arrays are assumed at the base station (BS) side.

Instead of considering *infinite* antenna arrays, we attempt to quantify the performance gap between the achievable sum-rate for ZF precoder and the broadcast channel (BC) capacity with *finite* BS antennas and give useful suggestions for practical deployment. Note that the same comparison for block-diagonalization (BD) scheme in MU-MIMO system can refer to [12].

In this article, we use the uncorrelated Rayleigh fading channel for theoretical derivation, which can closely model the large antenna spacing and rich scattering environment. Assuming perfect CSI is available, a lower bound of the performance gap aforementioned is provided. Using this bound, we first prove that the required number of BS antenna to achieve at least η% of the BC capacity is monotone decreasing with the increase of the transmit SNR. Then the largest number of BS antennas needed to reach a fixed percentage of the BC capacity is derived by exploiting the aforementioned monotonicity. Finally, we verified the theoretical derivation through simulation and evaluate the performance of ZF precoding in realistic propagation environments by conducting two measurements of massive MIMO in urban microcell (UMi) scenario with the frequencies of 3.5 GHz and 6 GHz.

Most of the measurement results are consistent with the theoretical derivation, except the condition of antennas with small element spacing in low transmitting signal-to-noise ratio (SNR), which beyond the uncorrelated Rayleigh channel models that we assumed in theoretical derivation. The measurement results also show that the ZF performance is better with larger antenna element spacing and higher frequency.

The remainder of this article is outlined as follows. In Section 2, the experimental set-up is described. In Section 3, we give the system model and performance metrics. In Section 4, we derive the interference moments and present results of interference against AS and antenna spacing. In Section 4, theoretical derivation of the needed number of the BS antennas for ZF precoder is given. In Section 4, simulations and real measurement results are demonstrated. Then, conclusions are drawn in Section 5.

Notations. Boldface lower and upper case symbols denote vectors and matrices, respectively. $\mathbb{C}^{m\times n}$ and $\mathbb{D}_K$ denote a complex matrix of dimension $m \times n$ and a diagonal matrix of dimension $K \times K$, respectively. $\|\cdot\|_F$ represents the Frobenius norm. The transpose, Hermitian transpose, and matrix inverse operators are represented by $(\cdot)^T$, $(\cdot)^H$, and $(\cdot)^{-1}$, respectively. We use $\mathbf{I}_N$ to denote the size-N identity matrix. $\mathbb{E}\{\cdot\}$, $\mathbf{Tr}\{\cdot\}$, and $det(\cdot)$ denote the expectation operator, the trace operator, and the determinant operator, respectively. We use $[\mathbf{A}]_{k,}$, $[\mathbf{A}]_{,m}$, and $[\mathbf{A}]_{km}$ to represent the vector of the k-th row, the vector of the m-th column, and the element of the k-th row m-th column of matrix $\mathbf{A}$, respectively.

2. Channel Measurement

2.1. Measurement System. To evaluate the performance of ZF precoding in the realistic propagation environment, extensive channel measurements were performed at the campus of Beijing University of Posts and Telecommunications (BUPT), China. With time domain multiplexed switching antennas in both transmitting terminal (Tx) and receiving terminal (Rx), the Elektrobit PropSound Channel Sounder can transmit periodic pseudo-random binary signals in the channel on a time division way [13], which ensures that each antenna element is independent of each other in multiantenna channel measurement.

Figures 1(a) and 1(b) show the layouts of antennas used in the measurement. The detailed configuration of antennas is given in Table 1. The Rx layout and schematic are shown in Figure 1(a). $1\sharp \sim 16\sharp$ elements were used in the 3D dual-polarized omnidirectional array (ODA) antenna as the user terminal. The Tx layout and schematic are shown in Figure 1(b). Dual-polarized uniform planar array (UPA) with 32 antenna elements is used at the Tx to set up a virtual massive MIMO antenna which includes 256 elements. The arrows in Figure 1(c) indicate the serial number of the antenna's movement position; by shifting the UPA horizontally and vertically 8 times as arrows show, we get an antenna matrix with 256 elements. In addition, Tx was put in one position till the raw data was collected; then it shifts to the other position

Table 1: Antenna configuration.

Type		Parameter values	
Antenna type		UPA	ODA
Element number		32	56(1♯ ~ 16♯ in use)
Cross polarization		±45°	±45°
Center frequency		3.5 GHz/6 GHz	3.5 GHz/6 GHz
Bandwidth		200 MHz	200 MHz
Distribution of antennas		planar	cylinder
Element spacing		0.5 wavelength	0.5 wavelength
Angle range	Azimuth	−70° ~ 70°	−180° ~ 180°
	Elevation	−70° ~ 70°	−55° ~ 90°

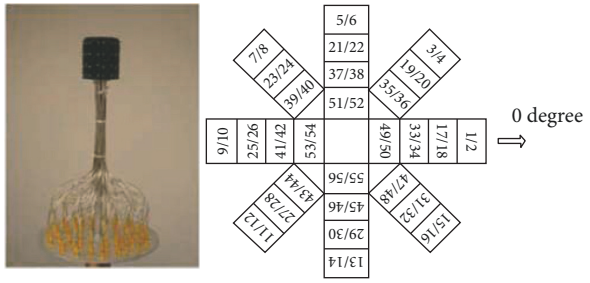

(a) Layout and schematic of ODA in Rx

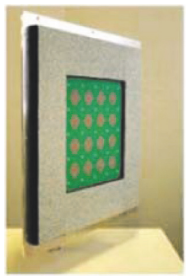

1/2	3/4	5/6	7/8
9/10	11/12	13/14	15/16
17/18	19/20	21/22	23/24
25/26	27/28	29/30	31/32

(b) Layout and schematic of UPA in Tx

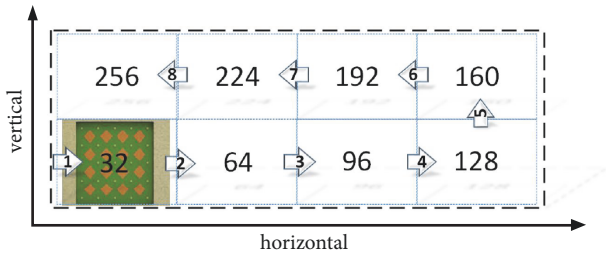

(c) Schematic diagram of 256 elements antenna in Tx

Figure 1: Layout and schematic of antenna array.

in one-point measurement. The campaigns are performed during school summer vacation; at that time few occurring moving objects and human bodies are on campus, so that a scatters static environment is assumed when we shift the 32-element UPA 8 times within a very short period. Thus, a time quasi-stationary environment is guaranteed, and the rationality of this virtual measurement method is ensured [14].

2.2. Measurement Scenario. The measurement campaigns are conducted around the Baoweichu Building of BUPT that is with much higher surrounding buildings, which forms a typical UMi scenario. As is shown in Figure 2(a) the red symbol denotes the location of the Tx antenna and yellow section denotes its 3 dB lobe width. The white points are Rx position. We choose the measurement data in NLoS positions 5 and 8 for analysis. As can be seen from Figure 2(b), the base station (as the Tx side) is located on the top of a 3-floor building with the height of 14.4 m. The mobile station (as the Rx side) is planned on the ground with the height of 1.9 m.

3. System Model

3.1. System Model. We consider a downlink MU-MIMO system with one base station (BS) equipped with M antennas that simultaneously serves K active independent single-antenna users. To guarantee the effectiveness of the communication, M is assumed more than K ($M > K$). At the BS, the transmitted symbols are assumed to be successively processed by a normalized power allocation matrix $\mathbf{\Lambda} \in \mathbb{D}_K$ satisfying $\mathbf{Tr}\{\mathbf{\Lambda}\mathbf{\Lambda}^H\} = 1$ and then by a normalized precoder $\mathbf{F}$ of dimension $M \times K$ satisfying $\|\mathbf{F}\|_F^2 = K$. We assume a narrowband flat fading channel model and obtain the received signal of the k-th user

$$y_k = \mathbf{g}_k \mathbf{F} \mathbf{\Lambda} \mathbf{s} + n_k \tag{1}$$

where $\mathbf{s}_k$ is the k-th elements of the normalized $\mathbf{s} \in \mathbb{C}^{K\times 1}$ satisfying $\mathbb{E}[\mathbf{s}\mathbf{s}^H] = (p_u/K)\mathbf{I}_K$, which denotes the information symbol to be transmitted to the k-th user. $\mathbf{g}_k = \mathbf{h}_k\sqrt{\beta_k} \in \mathbb{C}^{1\times M}$ models the downlink channel of the k-th user, where $\sqrt{\beta_k}$ models the large scale fading and $\mathbf{h}_k \in \mathbb{C}^{1\times M}$ models uncorrelated Rayleigh fast fading, which usually holds for large antenna spacing and rich scattering environment that is assumed to be i.i.d. RV with zero mean and unit variance. The channel matrix $\mathbf{G} \in \mathbb{C}^{K\times M}$ satisfying $[\mathbf{G}]_{k\cdot} = \mathbf{g}_k$ then equals $\mathbf{D}^{1/2}\mathbf{H}$, where $[\mathbf{H}]_{k\cdot} = \mathbf{h}_k$ and $\mathbf{D} \in \mathbb{D}_K$ satisfies $[\mathbf{D}]_{kk} = \beta_k$. We take $n_k \sim \mathcal{CN}(0,1)$ to be the normalized additive white Gaussian noise (AWGN) of the k-th user and $p_u > 0$ represents the average transmit SNR. Since the Rayleigh channel is rich scattering, we define the degree of freedom

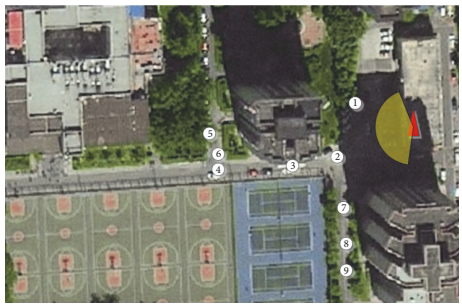

(a) The overview in UMi scenario

(b) The antenna position and environment

FIGURE 2: The overview of the measurement area by Baidu Map and the setup position of Tx and Rx antennas.

(DoF) to be the ratio of the number of BS antennas to that of users, which can be expressed as

$$\alpha = \frac{M}{K}. \tag{2}$$

3.2. ZF Precoder and BC Capacity. In this paper, we assume the BS has perfect CSI. If the transmitted symbols are processed by a ZF precoder, the precoding vector of the k-th user can be expressed as

$$\mathbf{f}_k = \frac{\mathbf{v}_k}{\|\mathbf{v}_k\|_F} \tag{3}$$

where $\mathbf{v}_k$ is the k-th column vector of the matrix $\mathbf{V}$ satisfying $\mathbf{V} = \mathbf{G}^H(\mathbf{G}\mathbf{G}^H)^{-1}$. When Gaussian symbols are transmitted, the ergodic sum-rate of the communication system using ZF precoder with the optimal power allocation can be expressed as

$$R_{ZF} = \mathbb{E}\left\{\sum_{k=1}^{K}\log_2\left(1 + \frac{p_u\Lambda_k}{K}\mathbf{g}_k\mathbf{f}_k\mathbf{f}_k^H\mathbf{g}_k^H\right)\right\}, \tag{4}$$

where $\Lambda_k = [\mathbf{\Lambda}\mathbf{\Lambda}^H]_{kk}$ and $\mathbf{\Lambda}$ is derived by waterfilling.

The BC capacity using the system model above can be further expressed as [15]

$$C_{sum} = \mathbb{E}\left\{\max_{\mathbf{\Lambda}:\mathbf{Tr}\{\mathbf{\Lambda}\mathbf{\Lambda}^H\}=1}\log_2 det\left(\mathbf{I}_K + \frac{p_u}{K}\mathbf{G}\mathbf{\Lambda}\mathbf{\Lambda}^H\mathbf{G}^H\right)\right\}. \tag{5}$$

We define γ as the ratio of the sum-rate of ZF precoder with the optimal power allocation to the BC capacity; i.e.,

$$\gamma = \frac{R_{ZF}}{C_{sum}}. \tag{6}$$

Typically, $\gamma = 1$ is achieved, using infinite BS antennas and allocating power with waterfilling, by massive MIMO effect.

4. How Many Antennas Do We Need?

In this section, we first evaluate ZF precoder with a finite number of BS antennas in terms of γ analysis, and then we prove how many antennas are needed at most to reach η% of the channel capacity with ZF precoder.

4.1. Lower Bound Analysis of γ. To begin with the analysis, we introduce the following lemmas.

Lemma 1. *The ergodic sum-rate of the communication system using ZF precoder with optimal power allocation for uncorrelated Rayleigh channel is lower bounded by*

$$\widehat{R}_{ZF} = \sum_{k=1}^{K}\log_2\left(1 + p_u(\alpha - 1)\beta_k\Lambda_k\right). \tag{7}$$

Proof. Substituting (3) into (4) and Using Jensen's inequality, the ergodic sum-rate of the communication system using ZF can be lower bounded as follows:

$$\begin{aligned} R_{ZF} &\geq \sum_{k=1}^{K}\log_2\left(1 + \frac{p_u\Lambda_k/K}{\mathbb{E}\left\{\|\mathbf{v}_k\|_F^2\right\}}\right) \\ &\overset{(a)}{=} \sum_{k=1}^{K}\log_2\left(1 + \frac{p_u\Lambda_k/K}{\mathbb{E}\left\{\left[\left(\mathbf{G}\mathbf{G}^H\right)^{-1}\right]_{kk}\right\}}\right) \\ &\overset{(b)}{=} \sum_{k=1}^{K}\log_2\left(1 + \frac{p_u(M-K)\beta_k\Lambda_k}{K}\right) \end{aligned} \tag{8}$$

where (a) is obtained exploiting the property $\|\mathbf{v}_k\|_F^2 = \mathbf{Tr}\{\mathbf{v}_k^H\mathbf{v}_k\}$ and (b) is acquired using the equation [[5], eq. (79)] $\mathbb{E}\{[(\mathbf{G}\mathbf{G}^H)^{-1}]_{kk}\} = 1/(M-K)\beta_k$. Substituting (2) into (8), we get (7). □

Lemma 2. *If the optimal power allocation is achieved, i.e., $\overline{\Lambda}_k = \mathrm{argmax}_{\mathbf{\Lambda}:\mathbf{Tr}\{\mathbf{\Lambda}\mathbf{\Lambda}^H\}=1}\log_2 det(\mathbf{I}_K + (p_u/K)\mathbf{G}\mathbf{\Lambda}\mathbf{\Lambda}^H\mathbf{G}^H)$, the channel capacity for uncorrelated Rayleigh channel of (5) is upper bounded by*

$$\widehat{C}_{sum} = \sum_{k=1}^{K}\log_2\left(1 + p_u\alpha\beta_k\overline{\Lambda}_k\right). \tag{9}$$

Proof. Exploiting the property of matrix determinant and Jensen's inequality, we have the BC capacity in (5) to be upper bounded by

$$\begin{aligned} C_{sum} &\le \mathbb{E}\left\{\sum_{k=1}^{K}\log_2\left(1+\frac{p_u\overline{\Lambda}_k}{K}\left[\mathbf{G}\mathbf{G}^H\right]_{kk}\right)\right\} \\ &\le \sum_{k=1}^{K}\log_2\left(1+\frac{p_u\overline{\Lambda}_k}{K}\mathbb{E}\left\{\left[\mathbf{G}\mathbf{G}^H\right]_{kk}\right)\right\} \\ &= \sum_{k=1}^{K}\log_2\left(1+\frac{p_u\overline{\Lambda}_k}{K}\frac{\beta_k}{K}\mathbb{E}\left\{\mathbf{Tr}\left\{\mathbf{H}\mathbf{H}^H\right\}\right)\right\} \\ &\overset{(a)}{=} \sum_{k=1}^{K}\log_2\left(1+\frac{p_uM\beta_k\overline{\Lambda}_k}{K}\right). \end{aligned} \tag{10}$$

where (a) is obtained by using $\mathbb{E}\{\mathbf{Tr}\{\mathbf{H}\mathbf{H}^H\}\} = MK$ [[16], Lemma 2.9]. Substituting (2) into (10), we derive (9). □

Combining Lemmas 1 and 2 derives the lower bound of γ as Proposition 3.

Proposition 3. *γ in (6) is lower bounded by*

$$\widehat{\gamma} = \frac{\sum_{k=1}^{K}\log_2\left(1+p_u(\alpha-1)\beta_k\overline{\Lambda}_k\right)}{\sum_{k=1}^{K}\log_2\left(1+p_u\alpha\beta_k\overline{\Lambda}_k\right)}. \tag{11}$$

Proof. From Lemma 1, we have the ZF's sum-rate of the optimal power allocation with Λ_k in (7) is no less than the power allocation with $\overline{\Lambda}_k$ in (9); i.e., $R_{ZF} \ge \widehat{R}_{ZF} \ge \sum_{k=1}^{K}\log_2(1+p_u(\alpha-1)\beta_k\overline{\Lambda}_k)$. From Lemma 2, we have $C_{sum} \le \sum_{k=1}^{K}\log_2(1+p_uM\beta_k\overline{\Lambda}_k/K)$. Combining all together, we can easily obtain the desired result. □

Now we can determine how many antennas is needed to reach at least η% of the channel capacity for ZF precoder with specified parameters, which satisfies the equation $\eta/100 = \sum_{k=1}^{K}\log_2(1+p_u(\alpha-1)\beta_k\overline{\Lambda}_k)/\sum_{k=1}^{K}\log_2(1+p_u\alpha\beta_k\overline{\Lambda}_k)$. For example, if the BS serves $K = 4$ users, when neglecting the large scale fading and power allocation, i.e., $\beta_k = 1, \overline{\Lambda}_k = 1/K$ for any K, and assuming $p_u = 0$ dB, the number of the needed BS antennas that lead ZF precoder to reach at least 90% of the channel capacity can be derived from solving the equation, which is equal to 27.

4.2. How Many Antennas Do We Need at Most? Although Proposition 3 provides a method to calculate the needed number of BS antennas with system parameters, it is complicated since it needs to know the large scale fading coefficients a prior, which may be changing throughout the communication procedure in some scenarios. Therefore, we derive an upper bound of the needed BS antennas that is only related to the objective percentage, η%, of the BC capacity and the number, K, of active users.

By analysing (11), we first present the following lemmas.

Lemma 4. *$\widehat{\gamma}$ in (11) is a monotone increasing function of the transmit SNR; i.e., $\forall p_u > 0$, we have*

$$\frac{d\widehat{\gamma}}{dp_u} > 0. \tag{12}$$

Proof. The derivative of $\widehat{\gamma}$ with respect to p_u can be expressed by

$$\begin{aligned} &\frac{d\widehat{\gamma}}{dp_u} \\ &= \frac{\sum_{k=1}^{K}P(\alpha-1,k)\sum_{k=1}^{K}Q(\alpha,k)}{\left[\sum_{k=1}^{K}Q(\alpha,k)\right]^2} \\ &\quad - \frac{\sum_{k=1}^{K}P(\alpha,k)\sum_{k=1}^{K}Q(\alpha-1,k)}{\left[\sum_{k=1}^{K}Q(\alpha,k)\right]^2} \\ &= \frac{\sum_{i=1,j=1}^{K}\left[P(\alpha-1,i)Q(\alpha,j)-P(\alpha,i)Q(\alpha-1,j)\right]}{\left[\sum_{k=1}^{K}Q(\alpha,k)\right]^2} \\ &= \frac{\sum_{i=1,j=1}^{K}\left[A(\alpha-1,i)T(\alpha,j)-A(\alpha,i)T(\alpha-1,j)\right]}{\left[\sum_{k=1}^{K}Q(\alpha,k)\right]^2 B(\alpha,i)B(\alpha-1,i)} \end{aligned} \tag{13}$$

where $P(x,m) = x\beta_m\overline{\Lambda}_m/(1+p_ux\beta_m\overline{\Lambda}_m)$, $Q(x,m) = \log_2(1+p_ux\beta_m\overline{\Lambda}_m)$, $A(x,m) = x\beta_m\overline{\Lambda}_m$, $B(x,m) = 1+p_ux\beta_m\overline{\Lambda}_m$, and $T(x,m) = B(x,m)Q(x,m)$ $(m = 1\cdots K)$. Since $M > K$, $\forall p_u > 0$ we have the following properties:

$$\alpha > \alpha - 1 > 0 \tag{14a}$$

$$A(\alpha,m) > A(\alpha-1,m) > 0 \tag{14b}$$

$$B(\alpha,m) > B(\alpha-1,m) > 1 \tag{14c}$$

$$Q(\alpha,m) > Q(\alpha-1,m) > 0. \tag{14d}$$

Taking the derivative of $T(x,m)$ with respect to p_u, we have

$$\frac{dT(x,m)}{dp_u} = A(x,m)Q(x,m) + A(x,m). \tag{15}$$

With the help of (15) and letting Z represent the numerator of (13), we get the derivative of Z with respect to p_u:

$$\begin{aligned} \frac{dZ}{dp_u} &= \sum_{i=1,j=1}^{K}\left[A(\alpha-1,i)\frac{dT(\alpha,j)}{dp_u}\right. \\ &\quad \left. - A(\alpha,i)\frac{dT(\alpha-1,j)}{dp_u}\right] \\ &= \sum_{i=1,j=1}^{K}\left[\alpha(\alpha-1)\right. \\ &\quad \left.\cdot\beta_i\beta_j\overline{\Lambda}_i\overline{\Lambda}_j\left(Q(\alpha,j)-Q(\alpha-1,j)\right)\right]. \end{aligned} \tag{16}$$

Since the large scale fading coefficients always have positive value, i.e., $\beta_k > 0$ for $k = 1\cdots K$, we can obtain $dZ/dp_u > 0$.

That is to say, Z is an monotone increasing function of p_u. $\forall p_u > 0$, we have

$$Z > \lim_{p_u=0} Z = 0. \tag{17}$$

Combining (17) and properties (14c) and (14d) together, we have both the numerator and the denominator of (13) to be positive values. Then we can easily get the desired result. □

Lemma 5. *The ratio of the sum-rate of ZF precoder with the optimal power allocation to the BC capacity will be lower bounded by $(\alpha - 1)/\alpha$ ($\alpha > 1$) that is independent of other system parameters, e.g., the transmit SNR and the large scale fading coefficients.*

Proof. Using Proposition 3, we have

$$\min \gamma \geq \min \widehat{\gamma}. \tag{18}$$

And using Lemma 4, we have $\min \widehat{\gamma}$ which is acquired with the smallest value of p_u. Then $\forall p_u > 0$, we obtain

$$\min \widehat{\gamma} = \lim_{p_u \longrightarrow 0} \widehat{\gamma}. \tag{19}$$

Further,

$$\begin{aligned} &\lim_{p_u \longrightarrow 0} \widehat{\gamma} \\ &\overset{(a)}{=} \lim_{p_u \longrightarrow 0} \frac{\sum_{k=1}^{K} \left((\alpha - 1) \beta_k \overline{\Lambda}_k / \left(1 + p_u (\alpha - 1) \beta_k \overline{\Lambda}_k \right) \right)}{\sum_{k=1}^{K} \left(\alpha \beta_k \overline{\Lambda}_k / \left(1 + p_u \alpha \beta_k \overline{\Lambda}_k \right) \right)} \\ &= \frac{\sum_{k=1}^{K} (\alpha - 1) \beta_k \overline{\Lambda}_k}{\sum_{k=1}^{K} \alpha \beta_k \overline{\Lambda}_k} = \frac{\alpha - 1}{\alpha} \end{aligned} \tag{20}$$

where (a) is obtained by using L'Hôspital's rule. Note that (20) is satisfied regardless of different p_u and β_k. Combining (18), (19), and (20) together, we derive the desired result. □

Then we derive the relationship between η% and M as Proposition 6.

Proposition 6. *The needed number, M, of BS antennas for ZF precoder to reach a fixed ratio, η%, of the BC capacity is monotone decreasing when the transmit SNR, p_u, is increased.*

Proof. With a similar procedure of Lemma 4, we can easily prove that $\widehat{\gamma}$ in (11) is also a monotone increasing function of the number of BS antennas. That is to say, both p_u and M will have a positive effect on $\widehat{\gamma}$. Therefore, M will decrease with increasing p_u when $\widehat{\gamma}$ is fixed to η%. Since the monotonicity is satisfied for both p_u and M on $\widehat{\gamma}$, the conclusion aforementioned will also satisfy the monotonicity. Then we derive the desired results. □

Finally, we give the conclusion about how many BS antennas are needed at most to reach a fixed percentage, η%, of the BC capacity that is only related to η and K as Proposition 7.

Proposition 7. *The largest number of the needed BS antennas for ZF precoder to achieve η% of the BC capacity is $100K/(100-\eta)$, which is independent of other system parameters.*

Proof. From Proposition 6, the largest needed number, M, of BS antennas is achieved when $p_u \longrightarrow 0$, which is exactly coincide with the situation described by Lemma 5. Therefore, the largest M can be derived by solving the equation $\eta/100 = (\alpha - 1)/\alpha$, which is independent of other system parameters. Then

$$\alpha = \frac{100}{100 - \eta}. \tag{21}$$

Comparing (2) with (21) can easily obtain the desired result. □

Proposition 7 has simplified the calculation of the largest number of the BS antennas; we need to deploy for reaching a certain percentage of the BC capacity without knowing the details about the system parameters but only the number of active users and the ultimate percentage. In addition, Proposition 6 indicates the trend of a monotonic reduced number of the needed BS antennas with an increasing transmit SNR; i.e., a lower number of BS antennas is needed for a higher transmit SNR.

5. Numerical Results

In order to confirm our theoretical derivation, simulation results are compared, and channel measurements are conducted for the evaluation of ZF precoding properties in realistic propagation environments. In the simulations of this section, we confirm our theory by validating some key propositions/lemmas. Firstly, Proposition 3 and Proposition 6 are validated by comparing γ to $\widehat{\gamma}$ with respect to the number of BS antennas for different SNR. And then Lemma 5 is confirmed by giving the curves of $\widehat{\gamma}$ with respect to the transmit SNR. In both simulations, the large-scale fading coefficient of each user is uniformly distributed in [0.5, 1.5]. In the first simulation, we assume that the BS serves $K = 4$ users. In addition, in both simulation and actual measurement, the ZF performances in three kinds of average transmit SNR conditions are compared, including 20 dB high SNR and 0 dB low SNR conditions in normal transmission environment and extreme conditions of -20 dB. And in the second one, the range of the average transmit SNR p_u is from −40 dB to 40 dB.

5.1. Simulation Results. Figure 3 shows the simulated and analytical lower bound of γ versus different numbers of BS antennas with different transmit SNR. From the figure, we can observe that the curves of the derived lower bound are relatively tight for every average transmit SNR, which confirms Proposition 3. In addition, we can observe from the figure that the needed number, M, of BS antennas for ZF precoder to reach at least a fixed percentage of the BC capacity decreases when the average transmit SNR is increased, e.g., $M \approx 40, 27$ and 12 for $p_u = -20$dB, 0dB and 20dB when η% = 90%, respectively, which further validates Proposition 6.

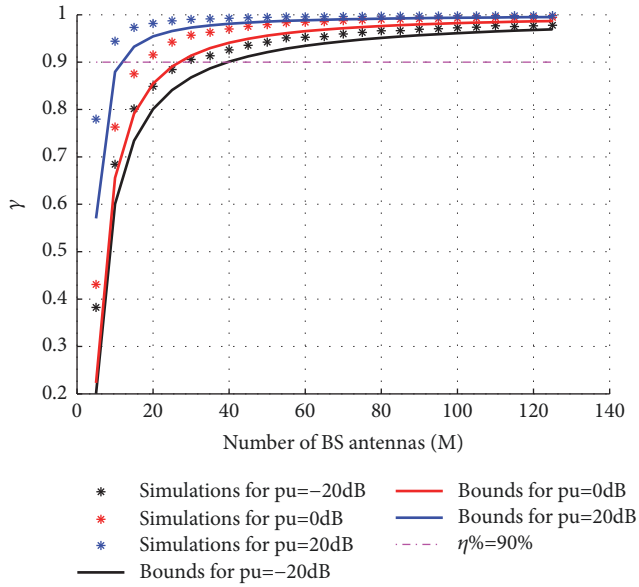

Figure 3: Lower bounds and numerically simulation results of γ versus different numbers of BS antennas with different transmit SNR.

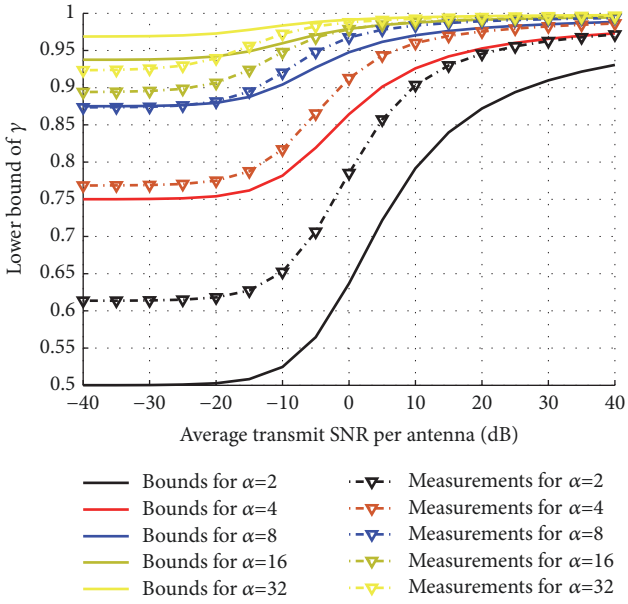

Figure 4: The 3.5 GHz measurement results and the lower bounds of γ with respect to the average transmit SNR for different DoF of the system.

Figure 4 shows the lower bound of γ versus increasing average transmit SNR with different DoF of the system. We can observe from the figure that all the curves are increasing functions of the average transmit SNR, which further supports Lemma 4. In addition, we can easily observe that the minimum performance of ZF for different α is exactly equal to $(\alpha-1)/\alpha$; e.g., the minimum performance of the red line is exactly equal to $(\alpha-1)/\alpha|_{\alpha=4} = (4-1)/4 = 0.75$, which confirms Lemma 5. With the confirmation of Proposition 6

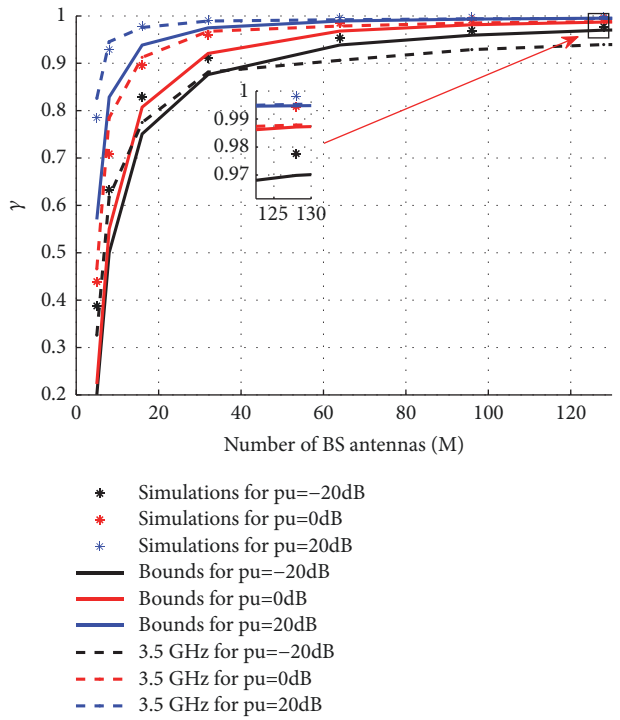

Figure 5: Simulation and 3.5 GHz measurement results of γ versus different numbers of BS antennas with different transmit SNR.

and Lemma 5, we can easily validate Proposition 7. Henceforth, all the propositions/lemmas in Section 4 are confirmed by our simulations.

5.2. Measurement Results. In order to evaluate the above theoretical derivation results in a realistic propagation environment, we conduct a massive MIMO channel measurement with 256 BS elements in the NLoS case of UMi scenario at two frequencies of 3.5 GHz and 6 GHz. The measurement environment is close to the noncorrelated Rayleigh channel model assumed in the derivation process. We reconstruct groups BS antennas with 5, 8, 16, 32, 64, 96, and 128 antenna elements from the measured CIR. In the reconstruction process, antenna elements are chosen far from each other to reduce the spatial correlation. However, due to the limitation of experimental conditions, as the number of selected elements increases, the element spacing from each other will be reduced. For example, when the element number is less than 8, the element spacing can be larger than 2 λ, but 1 λ spacing for the 32 elements antenna, and only 0.75 λ spacing for the antenna with 64 elements. Besides, a group of antennas with 0.5 λ spacing are extracted for the comparison of the above antennas.

Firstly, the performance of ZF at 3.5 GHz is analyzed.

As is shown in Figure 5, in normal transmission environment of SNR > 0 dB, the measurement results are better than the lower bound.

While at the extreme transmit conditions of SNR=-20 dB, there are two cases: when the antenna elements are less than 32 (element spacing $\geq 1\lambda$), the measurement results are

better than the bound; when the antenna elements is larger than 32 (element spacing $< 1\lambda$), the result is lower than the bound. This is because Lemma 5 and Proposition 7 are derived under the uncorrelated Rayleigh channel, and when, in extreme SNR, the correlation in the realistic propagation channel reaches a certain degree, there will be a clear gap between theoretical derivation and real measurement results, which indicates the performance of ZF precoding is more susceptible to the channel correlation in the case of extremely low SNR.

In addition, we choose a set of antennas with 0.5 λ spacing at 3.5 GHz for the comparison of ZF performance under different element spacing. As is shown in Figure 6, in the case of high SNR (20 dB), the channel correlation has little effect on the performance of ZF. The property of the antenna with small element spacing is slightly lower than that of the antenna with larger element spacing. And when SNR reduces, the performance gap between the antennas with two-element spacing increases obviously.

For the investigation of ZF performance versus increasing average transmit SNR with different DoF of the system in the real measured channels, the measured data are given in Figure 4. It can be seen that, in the case where the element spacing is larger than 1 λ (DoF $\alpha \leq 8$), the measured curve is above the derived lower bound, which is consistent with the result shown in Figure 5. That is, when the elements spatial correlation is smaller enough, the measured ZF performance is better than the lower bound. Limited by experimental conditions, as the number of selected antenna elements increases, the array element spacing decreases. When the element spacing is less than 1 λ, the performance of ZF is below the deduced lower bound at extremely low SNR (SNR < 0 dB). But when SNR increases, the gap decreases gradually. From [17] we can know that the correlation between array elements still exists when the antenna spacing is greater than 1 λ. Therefore, considering the antenna structure with reasonable spacing in the antenna designing can reduce the spatial correlation and improve the system performance of multiuser MIMO.

Since the rich dispersion of arrival angle at 6 GHz will make the spatial correlation lower and bring higher capacity [18], the performance of ZF precoding at 6 GHz is given in Figure 7 for the comparison of 3.5 GHz. The 6 GHz antenna has the same configuration as the 3.5 GHz antenna, that is, the same element number and the same $''\lambda''$ spacing [19]. It is clear that the ZF performances of 6 GHz are closer to the simulation results under the uncorrelated Rayleigh channel, which is better than 3.5 GHz one; i.e., at low SNR of -20 dB, the 6 GHz performance is lower than the bound only when the element spacing is less than 0.7 λ.

In addition, Figure 8 reflects in more detail of the enhancing of ZF precoding performance after increasing the frequency. It can be seen that as $\alpha = 8$, the performance of 6 GHz is already higher than the deduced bound; however, when the $\alpha = 16$ and 32, the property is below the lower bound at low SNR. The impact of correlation is still remarkable. However, in general, ZF precoding performance is significantly improved at a higher carrier frequency. This also illustrates from another aspect that the propagation channel with the 6 GHz carrier frequency is closer to the uncorrelated Rayleigh channel than the 3.5 GHz.

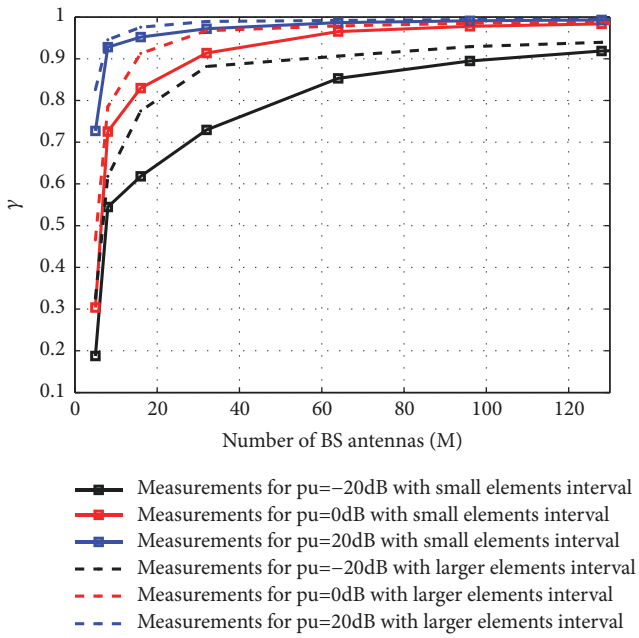

Figure 6: Measurement result with different element spacing.

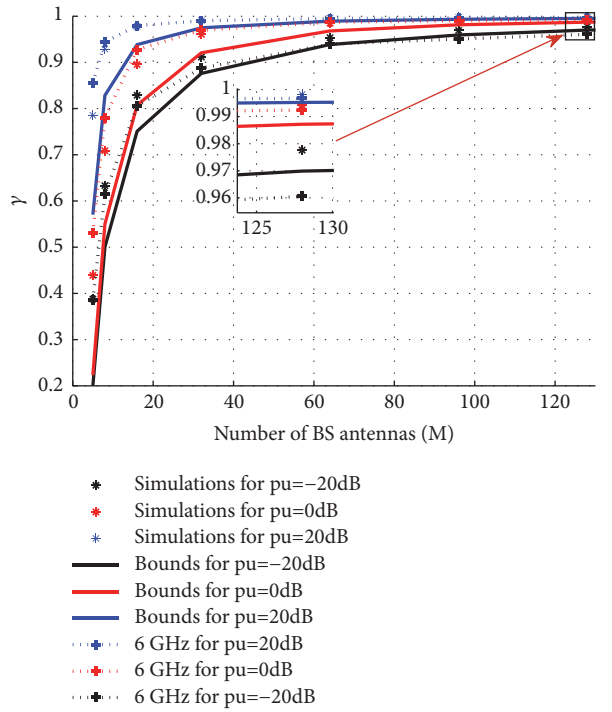

Figure 7: Simulation and 6 GHz measurement results of γ versus different numbers of BS antennas with different transmit SNR.

6. Conclusion

This paper has quantified the effect of a *finite* number of BS antennas on the sum-rate performance of ZF precoder in a

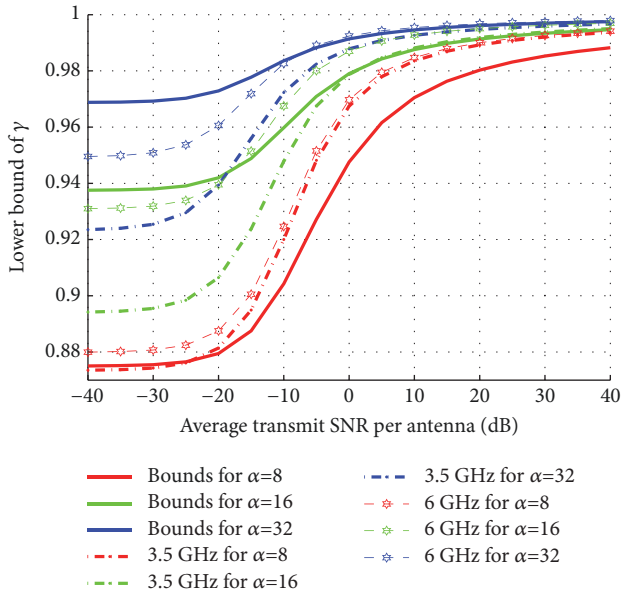

FIGURE 8: 3.5 GHz and 6 GHz measurement results of γ with respect to the average transmit SNR for different DoF of the system.

rich scattering channel from the theoretical derivation and channel measurement. Two insights have been derived from the theoretical analysis. (i) The needed number of the BS antennas for ZF precoder with the optimal power allocation to achieve at least η% of the BC capacity is monotone decreasing when the transmit SNR is increased. (ii) The needed antenna elements $M = 100K/(100 - \eta)$ which is only related to the ultimate percentage and the number of active users.

We verified the above theoretical derivation through simulation results and evaluate the properties through channel measurement in UMi scenario with frequencies of 3.5 and 6 GHz.

From the measurement results, as the antenna element spacing getting smaller, the correlation between channels increases, and the performance of ZF decreases. Besides, the transmission SNR has a great influence on the performance of ZF. Firstly, the performance of ZF is monotone increased with the increasing of transmitting SNR. Secondly, under normal transmit condition (SNR > 0 dB), the ZF performance is above the boundary, but, in extremely low SNR, when the element spacing is too small, e.g., the interval is less than 1λ in 3.5 GHz, it will be lower than the bound. This is because the extreme transmission condition is far from the Rayleigh noncorrelated channels that we assumed in the derivation.

In addition, we found that the performances of ZF precoding at 6 GHz is better than that of 3.5 GHz, in which results are closer to the theoretical derivation. Therefore, when the massive MIMO channel does not meet the favorable propagation state, improving the SNR and increasing the antenna element spacing or choosing a more suitable frequency can effectively enhance the sum-rate performance of ZF precoding. The conclusion provides a theoretical boundary and a reference of actual propagation performance for practical massive MIMO antenna deployment.

Data Availability

The raw data used to support the findings of this study were supplied by BUPT-RTT2 under license and so cannot be made freely available. Requests for access to these data should be made to professer Jianhua Zhang, jhzhang@bupt.edu.cn.

Conflicts of Interest

The authors declare that there are no conflicts of interest regarding the publication of this paper.

Acknowledgments

This research is supported by National Science and Technology Major Program of the Ministry of Science and Technology (no. 2018ZX03001031), Key Program of Beijing Municipal Natural Science Foundation (no. L172030), Beijing Municipal Science & Technology Commission Project (no. Z181100003218007), Key Project of State Key Lab of Networking and Switching Technology (NST20170205), and National Key Technology Research and Development Program of the Ministry of Science and Technology of China (no. 2012BAF14B01). This research is also supported by Huawei Technologies Co., Ltd. An earlier version of this paper was presented at the International Conference on 2018 IEEE 29th Annual International Symposium on Personal, Indoor and Mobile Radio Communications (PIMRC).

References

[1] J. G. Andrews, S. Buzzi, W. Choi et al., "What will 5G be?" *IEEE Journal on Selected Areas in Communications*, vol. 32, no. 6, pp. 1065–1082, 2014.

[2] M. Shafi, J. Zhang, H. Tataria et al., "Microwave vs. millimeter-wave propagation channels: key differences and impact on 5G cellular systems," *IEEE Communications Magazine*, vol. 56, no. 12, pp. 14–20, 2018.

[3] F. Rusek, D. Persson, B. K. Lau et al., "Scaling up MIMO: opportunities and challenges with very large arrays," *IEEE Signal Processing Magazine*, vol. 30, no. 1, pp. 40–60, 2013.

[4] T. L. Marzetta, "Noncooperative cellular wireless with unlimited numbers of base station antennas," *IEEE Transactions on Wireless Communications*, vol. 9, no. 11, pp. 3590–3600, 2010.

[5] J. Hoydis, S. Ten Brink, and M. Debbah, "Massive MIMO in the UL/DL of cellular networks: how many antennas do we need?" *IEEE Journal on Selected Areas in Communications*, vol. 31, no. 2, pp. 160–171, 2013.

[6] H. Q. Ngo, E. G. Larsson, and T. L. Marzetta, "The multicell multiuser MIMO uplink with very large antenna arrays and a finite-dimensional channel," *IEEE Transactions on Communications*, vol. 61, no. 6, pp. 2350–2361, 2013.

[7] C. Masouros, J. Chen, K. Tong, M. Sellathurai, T. Ratnarajah, and J. Wang, "Large scale antenna arrays with increasing antennas in limited physical space," *China Communications*, vol. 11, no. 11, pp. 7–15, 2014.

[8] C. Masouros and M. Matthaiou, "Space-constrained massive MIMO: hitting the wall of favorable propagation," *IEEE Communications Letters*, vol. 19, no. 5, pp. 771–774, 2015.

[9] X. Gao, O. Edfors, F. Rusek, and F. Tufvesson, "Linear precoding performance in measured very-large MIMO channels," in *Proceedings of the IEEE Vehicular Technology Conference (VTC Fall '11)*, pp. 1–5, IEEE, San Francisco, Calif, USA, September 2011.

[10] H. Q. Ngo, E. G. Larsson, and T. L. Marzetta, "Energy and spectral efficiency of very large multiuser MIMO systems," *IEEE Transactions on Communications*, vol. 61, no. 4, pp. 1436–1449, 2013.

[11] H. Q. Ngo, M. Matthaiou, T. D. Duong, and E. G. Larsson, "Uplink performance analysis of multicell MU-SIMO systems with ZF receivers," *IEEE Transactions on Vehicular Technology*, vol. 62, no. 9, pp. 4471–4483, 2013.

[12] Z. Shen, R. Chen, J. G. Andrews, R. W. Heath Jr., and B. L. Evans, "Sum capacity of multiuser MIMO broadcast channels with block diagonalization," *IEEE Transactions on Wireless Communications*, vol. 6, no. 6, pp. 2040–2045, 2007.

[13] J. Zhang, "Review of wideband MIMO channel measurement and modeling for IMT-Advanced systems," *Chinese Science Bulletin*, vol. 57, no. 19, pp. 2387–2400, 2012.

[14] H. Yu, J. Zhang, Q. Zheng, Z. Zheng, L. Tian, and Y. Wu, "The rationality analysis of massive MIMO virtual measurement at 3.5 GHz," in *Proceedings of the 2016 IEEE/CIC International Conference on Communications in China, ICCC Workshops 2016*, pp. 1–5, China, July 2016.

[15] P. Viswanath and D. N. C. Tse, "Sum capacity of the vector Gaussian broadcast channel and uplink-downlink duality," *IEEE Transactions on Information Theory*, vol. 49, no. 8, pp. 1912–1921, 2003.

[16] A. M. Tulino, *Random Matrix Theory And Wireless Communications*, Now Publishers Inc., 2004.

[17] Z. Zhe, T. Lei, and Z. Jianhua, "Elevation spatial characteristic investigation based on 3D massive MIMO channel measurements at 6 GHz," *Journal of China Universities of Posts and Telecommunications*, vol. 25, no. 3, pp. 1–91, 2018.

[18] J. Zhang, Z. Zheng, Y. Zhang, J. Xi, X. Zhao, and G. Gui, "3D MIMO for 5G NR: several observations from 32 to massive 256 antennas based on channel measurement," *IEEE Communications Magazine*, vol. 56, no. 3, pp. 62–70, 2018.

[19] J. Zhang, Y. Zhang, Y. Yu, R. Xu, Q. Zheng, and P. Zhang, "3-D MIMO: how much does it meet our expectations observed from channel measurements?" *IEEE Journal on Selected Areas in Communications*, vol. 35, no. 8, pp. 1887–1903, 2017.